

Investigation of the structural, optical and electrical properties of Nd-doped ZnO thin films deposited by spray pyrolysis

A. Douayar¹, P. Prieto², G. Schmerber⁵, K. Nouneh³, R. Diaz², I. Chaki¹, S. Colis⁵, A. El Fakir¹, N. Hassanain¹, A. Belayachi¹, Z. Sekkat³, A. Slaoui⁴, A. Dinia⁵, and M. Abd-Lefdil^{1,a,b}

¹ Université Mohammed V-Agdal, Faculté des Sciences, LPM, B.P. 1014, Rabat, Morocco

² Departamento de Física Aplicada C-XII, Universidad Autónoma de Madrid, Madrid, Spain

³ MASCIIR Moroccan Advanced Science, Innovation and Research Foundation, ENSET, Av. Armée Royale, Rabat, Morocco

⁴ InESS, UMR CNRS 7163 UDS, 23 rue du Loess, B.P. 43, 67037 Strasbourg, France

⁵ IPCMS, UMR CNRS 7504 UDS-ECPM, 23 rue du Loess, B.P. 43, 67034 Strasbourg, France

Received: 24 September 2012 / Received in final form: 13 December 2012 / Accepted: 2 January 2013
Published online: 31 January 2013 – © EDP Sciences 2013

Abstract. Neodymium-doped zinc oxide (NZO) thin films were deposited on glass substrates by spray pyrolysis technique. X-ray diffraction patterns have shown that both undoped and Nd-doped ZnO films exhibit the hexagonal wurtzite crystal structure with a preferential orientation along [0 0 2] direction. The effective doping concentration has been determined by Rutherford backscattering measurements showing that the neodymium is not incorporated easily into ZnO host matrix. The surface roughness was shown to increase with Nd doping. NZO films are highly transparent in the visible region. The lowest electrical resistivity value of about $4.0 \cdot 10^{-2} \Omega \text{ cm}$ was obtained for 1% Nd effective doping.

1 Introduction

Zinc oxide has attracted significant interest because of its nontoxic character, chemical stability, low cost and potential applications in many technological fields [1–6]. ZnO is known to be an *n*-type semiconductor with a wide band gap 3.35 eV at room temperature and a large exciton binding energy of about 60 meV [7]. Numerous techniques such as reactive evaporation, sputtering, pulsed laser deposition, sol-gel and spray pyrolysis were used for the growth of undoped and doped ZnO thin films [8–16]. It is well established that physical and chemical properties of ZnO can be largely modified upon doping [17–21]. Doping ZnO with rare earth ions was shown to lead to interesting optical and magnetic properties. ZnO films doped with Nd (0.01, 0.1 or 1% Nd) grown on a plane sapphire or fused silica substrates by pulsed laser deposition [21] showed a pronounced negative magnetoresistance ratio which was attributed to a paramagnetic behavior of the Nd³⁺ ions. Other authors, such as Ungureanu et al. [22] who reported the influence of Nd doping on several properties of NZO films deposited on Si (1 0 0) by spray pyrolysis, showed that the samples exhibit ferromagnetic properties at room temperature. More recently, the existence of robust ferromagnetic properties associated with a strong anisotropy was evidenced in NZO nanowires, suggesting that such

material could be used in spintronic applications [23]. In all cases the recorded magnetization remained small and showed finally the same discrepancies as those reported in transition metal doped ZnO [24,25]. From the optical point of view, rare earth ions have always shown an interesting optical activity when used as dopant in oxide matrices. More precisely, such doped oxides can be used as downshifting and/or conversion layers within photovoltaic solar cells in order to improve their efficiency. Optical measurements have already shown that the near edge band position of ZnO shifts toward higher wavelengths due to the substitution of Nd for Zn [23]. It was also suggested that this shift is related to the annealing temperature and that smaller shift is obtained at high temperature [26]. For NZO prepared by sol-gel method [27], different time evolutions and decay behaviors of $^4F_{3/2} \rightarrow ^4I_{11/2}$ of Nd³⁺ ions were observed by employing time-resolved laser spectroscopy, which was attributed to the existence of multiple luminescence centers of Nd³⁺ ions with various PL lifetimes.

In the present work, NZO thin films were deposited on glass substrates by spray pyrolysis technique. The Nd effect on the structural, optical and electrical properties is analyzed. The aim of the study is to check the evolution of the optical properties with the Nd concentration and its relation to the sample conductivity (i.e., carrier concentration and mobility). Different Nd concentrations up to 5% are tested in order to evaluate the solubility limit of this ion inside the ZnO host lattice.

^a e-mail: a-lefdil@fsr.ac.ma

^b e-mail: mabdlefdil@gmail.com

2 Experimental details

Undoped and Nd-doped ZnO films have been deposited on glass substrates by spray pyrolysis technique. A homogeneous solution was prepared by dissolving zinc chloride (ZnCl_2) (0.05 M) and hexahydrated neodymium chloride ($\text{NdCl}_3 \cdot 6\text{H}_2\text{O}$) in distilled water at room temperature. The solutions have 0, 1, 3 and 5 at.% Nd molar ratio. Some drops of acetic acid (CH_3COOH) have been added while stirring at room temperature for 30 min to obtain a clear solution. The glass substrate was cleaned in ethanol, rinsed in distilled water and subsequently dried under a nitrogen gas flow before deposition.

The substrate temperature was maintained constant at 350 °C. The structure of the films was investigated by X-ray diffraction (XRD) using a X'Pert Pro diffractometer with Cu K_α radiation ($\lambda = 1.54056 \text{ \AA}$). Rutherford backscattering spectrometry, using the 5 MV tandem accelerator of CMAM [28], has been used to determine the thickness and composition of the samples. A 3.045 MeV $^4\text{He}^+$ beam has been used to exploit the resonance with oxygen occurring at this energy [29]. Backscattered ions were detected using two surface barrier detectors in the horizontal plane at 170.5° and 165°. The samples were tilted by 7° with respect to the beam to decrease the energy straggling. The analysis of chemical composition along the sample thickness has been done by using simulation with SIMNRA code [30].

Optical transmittance $T(\lambda)$ and reflectance $R(\lambda)$ were obtained by means of a Cary 17D double-beam spectrophotometer. The absorption coefficient of each thin film has been computed using a model where the films thickness, the coherent multiple reflections in the film and the incoherent reflections in the substrate were considered. Photoluminescence (PL) measurements were also performed in order to have an insight into the film defects and into the possible spectral transitions of Nd^{3+} . For the PL experiment carried out at room temperature in the visible range, the 355 nm excitation line of a frequency-tripled neodymium-doped yttrium aluminum garnet Nd-YAG laser was used. The electrical properties of the films were studied at room temperature using an Ecopia Hall effect measurement system.

3 Results and discussion

Figure 1 shows the XRD patterns of undoped and Nd-doped ZnO thin films. All the observed diffraction peaks can be indexed according to the wurtzite structure of ZnO (JCPDS data [89-1397]). No additional peak corresponding to secondary phases could be observed within the detection limit of the XRD technique. The lattice parameters a and c of the different films have been determined using the formula: $d_{(h\ k\ l)} = \frac{a}{\sqrt{\frac{4}{3}(h^2+k^2+hk)+l^2\frac{a^2}{c^2}}}$. The values of a and c were found around 0.319 nm and 0.521 nm, respectively, which is in agreement with the usually published values for ZnO. A very small shift, close to the error bar of the XRD measurements, is observed which suggests

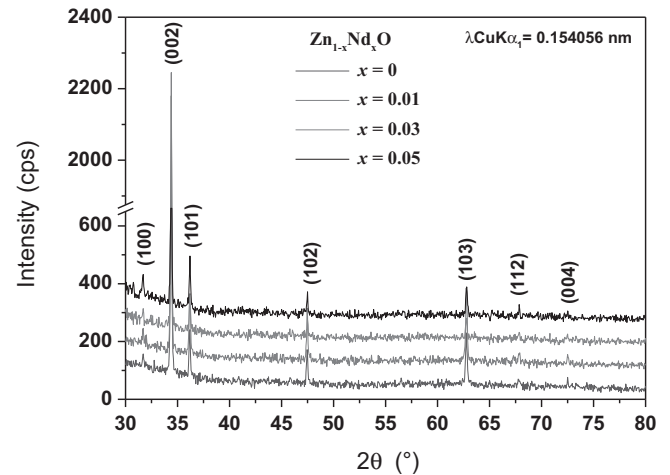


Fig. 1. XRD patterns of $\text{Zn}_{1-x}\text{Nd}_x\text{O}$ ($x = 0, 0.01, 0.03, 0.05$) thin films deposited by spray on glass substrates.

a very small increase of the lattice parameter upon Nd doping. The average crystallite sizes of the films have been estimated using the Scherrer's formula: $D = \frac{0.89\lambda}{\beta \cos \theta}$ where β is the full width at half maximum (FWHM) and λ is the X-ray wavelength. The crystallite sizes D in films were in the 70–85 nm range, which corresponds to the coherence length along the growth direction. A close look at Table 1 suggests that the grain size first decreases when 1% of Nd is inserted in the matrix, while for larger concentrations it increases again at values even larger than those recorded for the undoped sample. The decrease in the grain size is often attributed to the fact that impurities constitute nucleation centers. Moreover, if we keep in mind that the size of the Nd^{3+} ion is much larger than that of Zn^{2+} we can easily understand the observed decrease in grain size. This is also frequently associated with an increased concentration of defects in such samples. However, in this vein, it is more difficult to interpret the increase of the grain size for Nd concentrations larger to 1%, unless we assume that the solubility limit for Nd in ZnO is smaller than 1%. Above this concentration value, it is possible that the Nd is no more inserted in the matrix but acts in reducing the interstitial oxygen and leading to the formation of small clusters of Nd_2O_3 , that are too small to be detected by XRD. This may explain the increase of the grain size. Note also that for Nd concentration of 1%, Xian and Li [31] found the best crystalline quality for NZO films obtained by sol-gel method. This suggests that the final properties of the Nd-doped ZnO layers are also strongly dependent on the preparation technique.

From the values of the grain size D the dislocation density δ , the number of crystallites per unit surface area N and the strain ε can be determined using the following equations [32]: $\delta = \frac{1}{D^2}$; $N = \frac{t}{D^3}$ and $\varepsilon = \frac{\beta \times \cos \theta}{4}$ where t is the film thickness. The value of dislocation density δ which represents the amount defects in the films seems constant but is lower than that obtained for ZnO grown by chemical bath deposition [33]. The texture coefficient (TC), which represents the texture of particular plane,

Table 1. Composition and structural parameters of NZO thin films.

x_{nominal}	RBS			XRD			
	$x_{\text{effective}}$	t (nm)	D (nm)	TC(0 0 2)	δ (lines μm^{-2})	N (μm^{-2})	ε (10^{-4})
0	0	410 ± 40	74	2.9	180	1000	4.7
0.01	0.005	373 ± 35	70	2.7	210	1100	5.0
0.03	0.010	314 ± 30	85	2.8	140	350	4.1
0.05	0.013	285 ± 25	85	3.0	140	300	4.1

was also estimated. The TC value of particular plan is defined by the relation: $\text{TC}(h k l) = \frac{I(h k l)/I_0(h k l)}{N^{-1} \sum_N I(h k l)/I_0(h k l)}$, where $I(h k l)$ is the measured relative intensity of a plane $(h k l)$, $I_0(h k l)$ is the standard intensity of the plane $(h k l)$ taken from JCPDS data [89-1397] and N is the number of diffraction peaks. Its deviation from unity indicates the possibility of preferential growth along the $[h k l]$ direction. TC(0 0 2) calculated values (see Tab. 1) confirm the preferred orientation along the $[0 0 2]$ direction. For all the samples, TC(0 0 2) remains constant indicating that the insertion of Nd does not modify the ZnO preferential growth orientation.

Figure 2 shows the experimental RBS spectra at scattering angle of 170.5° and 3.045 MeV He^+ for $\text{Zn}_{1-x}\text{Nd}_x\text{O}$ ($x = 0.01, 0.03$ and 0.05) thin films. The energies of the He atoms backscattered at the sample surface by the main elements present at the sample, i.e., O, Si, Zn and Nd, are indicated by arrows in the figure while the yield at lower energies is related to their concentration along the growth direction. There is also a smaller contribution of K and Ca from the glass substrate at energies of around 1.7 and 1.8 MeV respectively. The Nd intensity increases as expected with the nominal Nd concentration. In addition, both Zn and Nd peaks present a smooth variation in the lower energy region. This suggests the presence of an important interface roughness between the film and the substrate with respect to the films surfaces, which is still significant as evidenced by the slope of both Zn and Nd lines in the high energy part. We have also performed the simulation of the RBS spectra by using SIMNRA code in terms of different layers with gradual composition from the $\text{Zn}_{1-x}\text{Nd}_x\text{O}$ thin film to the glass substrate. The thickness and the Nd composition of the $\text{Zn}_{1-x}\text{Nd}_x\text{O}$ thin films estimated by using the areal densities of Zn and Nd in terms of atoms/cm² and the mass density of ZnO, i.e., 5.6 g/cm³, are shown in Table 1. It can be observed that the Nd concentration estimated by RBS is systematically lower than the nominal one. The difference between the nominal and the real concentration increases with increasing the nominal concentration. This is clearly evidenced in the inset of Figure 2 where the Nd signal has been amplified to make the understanding easier for the reader. This can be explained by the low solubility limit of Nd in ZnO with respect to the case of Yb as previously observed in $\text{Zn}_{1-x}\text{Yb}_x\text{O}$ thin films [18]. Indeed, the solubility of Nd^{3+} ion is expected to be much lower than that of Yb^{3+} , in relation to the ionic radii difference between these elements (Nd^{3+} : 0.99 Å and Yb^{3+} : 0.87 Å [34]).

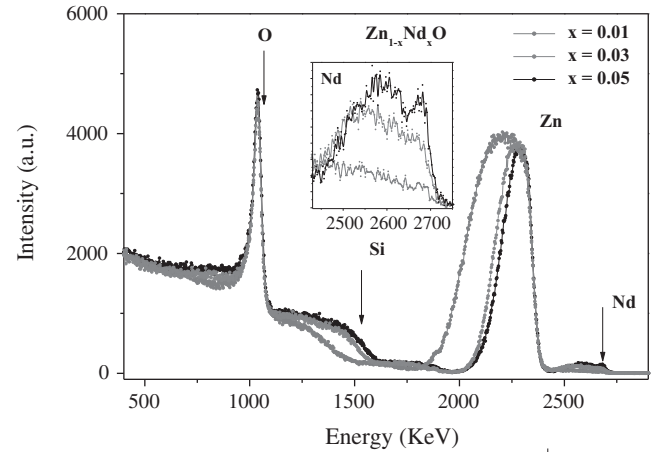


Fig. 2. RBS spectra of the $\text{Zn}_{1-x}\text{Nd}_x\text{O}$ thin films deposited on glass substrate. Inset: RBS spectra of ZnO thin film with its curve simulation.

Figure 3 shows the AFM images of Nd-doped ZnO films. It can be seen that all the samples have uniform and dense ZnO grains. The surface root mean square (rms) roughness is around 25 nm for undoped ZnO and increases with Nd doping to up to values around 40 nm. This is in agreement with the RBS spectra that showed a non-negligible slope in the high region part. The increase of the surface roughness is also compatible with the increase of the grain size as this has been evidenced in the XRD measurements.

Figure 4 shows $T(\lambda)$ and $R(\lambda)$ spectra of NZO thin films and the glass substrate transmittance. The films were highly transparent and the transmittance decreases when Nd doping increases. The absence of interference fringes in $T(\lambda)$ and $R(\lambda)$ spectra is related to the diffusion phenomenon, in agreement with the small grain size and the observed roughness. Qualitatively, it can be easily observed that the band gap changes upon Nd doping. In order to have more precise estimations on the gap value, the plots of $(\alpha h\nu)^2$ versus $h\nu$ are reported in Figure 5 for various Nd-doped ZnO samples. The extrapolation of the linear portion of the plots onto the energy axis gives the band gap value. A decrease from 3.22 eV down to 3.14 eV is observed when increasing the Nd concentration up to 5%. This is probably due to increase of Nd defects in the ZnO upon doping. According to Zheng et al. [35] Nd 4f electrons

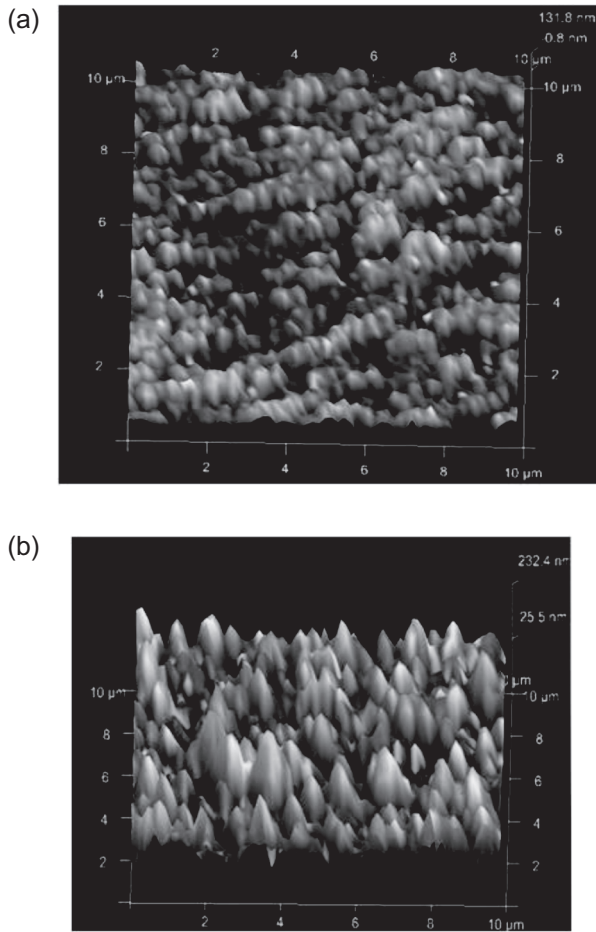


Fig. 3. AFM images of $\text{Zn}_{1-x}\text{Nd}_x\text{O}$ thin films deposited by spray on glass substrates: (a) $x = 0$ and (b) $x = 0.05$.

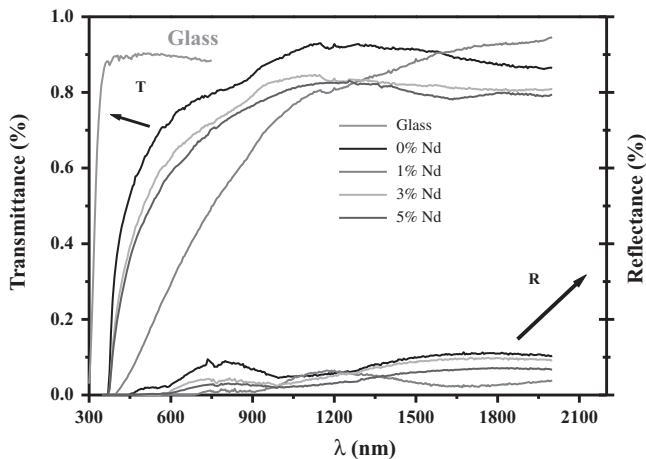


Fig. 4. Transmission and reflectance UV-NIR spectra of $\text{Zn}_{1-x}\text{Nd}_x\text{O}$ thin films deposited by spray on glass substrates.

introduce new states close to the conduction band of ZnO. A newer LUMO is therefore formed which leads to a reduction of the band gap. Note that such decrease in the gap is in agreement with the red shift of the excitonic peak observed in photoluminescence measurements for Nd-doped

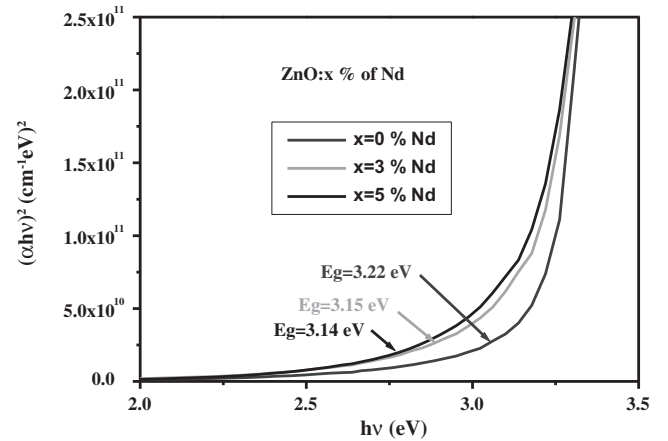


Fig. 5. $(\alpha h\nu)^2$ versus $h\nu$ of undoped and Nd-doped ZnO thin films deposited on glass substrate.

ZnO [23,35] and in other transition metal doped ZnO films grown by spray and other techniques [12,36–38].

Photoluminescence spectra, recorded at room temperature for NZO thin films, are reported in Figure 6. Except the laser lines (at 355 nm and its second order at 710 nm), two main lines are observed on the spectra. The strong luminescence band at 379 nm corresponds to the excitonic emission, i.e., to the recombination of electron and hole across the gap of the sample. The second order of this PL band is visible at 760 nm. As explained above, a small red shift is observed when increasing the Nd concentration. The second line is a wide PL band between 510 and 680 nm, characteristic of deep levels of oxygen vacancies in the ZnO matrix and zinc or oxygen atoms in interstitial position [39]. It is important to point out that in the doped samples this line is almost absent which suggests that, the increase of the Nd concentration leads to a reduction of radiative defects like oxygen vacancies or interstitial. This is in agreement with XRD analysis. Note that such healing of the ZnO native defects strongly depends on the nature of the doping ion. Indeed this phenomenon is almost absent in Yb-doped ZnO thin films grown by the same deposition technique [18]. No emission from Nd^{3+} ions is observed in the 400–1000 nm wavelength range indicating that there is no energy transfer from ZnO into Nd^{3+} ions in our samples.

For NZO thin films, carriers originate from both intrinsic donors such as lattice defects (oxygen vacancies and metal atoms in interstitial positions) and extrinsic doping due to the substitution of Nd for Zn in ZnO matrix. One hole will be produced for every Zn^{2+} substitution by Nd^{3+} , which will contribute to the electric conduction of the films as free carriers. Therefore, NZO films are expected to present a lower conductivity due to the compensation of the n -type carriers naturally presented in undoped ZnO with the holes introduced by the Nd^{3+} dopant. This is in agreement with the increase of the resistivity (decrease of the carrier concentration) when doping ZnO with 1% of Nd (Tab. 2). For larger Nd concentrations, the resistivity decreases again and the n -type character is reinforced (increase of the carrier concentration). This suggests that further doping does not lead to

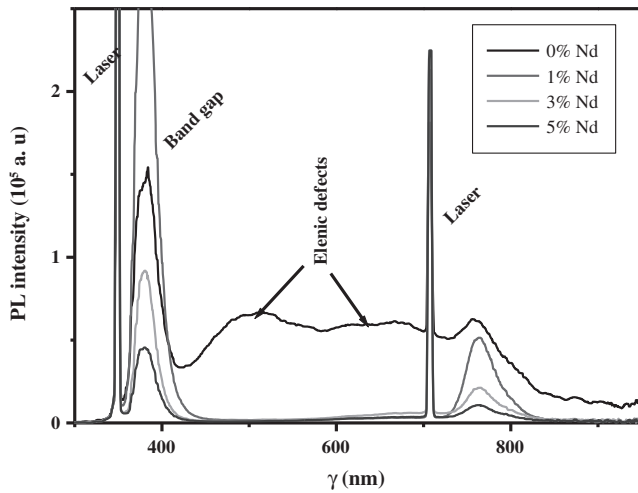


Fig. 6. Photoluminescence at room temperature in the visible region of $\text{Zn}_{1-x}\text{Nd}_x\text{O}$ thin films deposited on glass substrate.

Table 2. Electrical parameters of NZO thin films.

x_{nominal}	Hall effect		
	N (10^{20} cm^{-3})	ρ ($\Omega \text{ cm}$)	μ ($\text{cm}^2/\text{V s}$)
0	0.13	0.70	0.68
0.01	0.10	1.44	0.42
0.03	1.87	0.04	0.90
0.05	7.41	0.03	0.25

an increase of Nd ions in substitution of the Zn ions, but to the appearance of new defects (not necessarily optically active) and to spurious phases (such as Nd_2O_3 which was reported in highly doped ZnO samples [35] that increase further the n -type conduction. These results are in agreement with both XRD and photoluminescence results. A synthesis of the Hall effect results is presented in Table 2 where the best values of electrical resistivity and carriers mobility are about $4.0 \cdot 10^{-2} \Omega \text{ cm}$ and $0.90 \text{ cm}^2/\text{V s}$ respectively obtained for 1% effective (3% nominal) Nd doping. Such results are in agreement with those recently reported in Nd-doped SnO_2 thin films [40].

4 Conclusion

We have succeeded to grow polycrystalline $\text{Zn}_{1-x}\text{Nd}_x\text{O}$ films by pyrolysis technique. The structure of the films is not sensitively modified by incorporation of Nd. From RBS measurements, it is found that the neodymium is not homogeneously distributed in the whole ZnO matrix. X-ray diffraction and optical measurements suggested that the Nd solubility is small. The photoluminescence measurement has showed a decrease in the band gap with Nd doping but no emission in the visible range due to Nd ions. The films were highly transparent and the lowest electrical resistivity was around $4.0 \cdot 10^{-2} \Omega \text{ cm}$ obtained for 1% effective doping.

References

1. Z. Fan, D. Wang, P. Chang, W. Tseng, J.E. Lu, Appl. Phys. Lett. **85**, 5932 (2004)
2. M.A. Contreras, B. Egaas, K. Ramanathan, J. Hiltner, A. Swartzlander, F. Hasoon, R. Noufi, Prog. Photovolt. Res. Appl. **7**, 311 (1999)
3. Q. Wan, Q.H. Li, Y.J. Chen, T.H. Wang, X.L. He, J.P. Li, C.L. Lin, Appl. Phys. Lett. **84**, 3654 (2004)
4. E.M.C. Fortunato, P.M.C. Barquinha, A.C.M.B.G. Pimental, A.M.F. Goncalves, A.J. Marques, L.M.N. Pereira, R.F.P. Martins, Adv. Mat. **17**, 590 (2005)
5. T. Trupke, M.A. Green, P. Würfel, J. Appl. Phys. **92**, 1668 (2002)
6. J. Petersen, C. Brimont, M. Gallart, O. Crégut, G. Schmerber, O. Gilliot, B. Hönerlage, C. Ulhaq-Bouillet, J.L. Rehspringer, C. Leuvrey, S. Colis, A. Slaoui, A. Dinia, J. Appl. Phys. **104**, 113539 (2008)
7. A.B. Djurišić, A.M.C. Ng, X.Y. Chen, Prog. Quant. Electr. **34**, 191 (2010)
8. J.S. Oyola, J.M. Castro, G. Gordillo, Solar Energy Mater. Solar Cells **102**, 137 (2012)
9. Y. Belghazi, G. Schmerber, S. Colis, J.L. Rehspringer, A. Berrada, A. Dinia, J. Magn. Magn. Mater. **310**, 2092 (2007)
10. H. Zhu, J. Hüpkens, E. Bunte, J. Owen, S.M. Huang, Solar Energy Mater. Solar Cells **95**, 964 (2011)
11. I. Soumahoro, R. Moubah, G. Schmerber, S. Colis, M. Ait Aouaj, M. Abd-lefdil, N. Hassanain, A. Berrada, A. Dinia, Thin Solid Films **518**, 4593 (2010)
12. S. Tripathi, R.J. Choudhary, A. Tripathi, V. Branwa, A.C. Pandey, J.W. Gerlach, C. Dar, D. Kanjilal, Nucl. Instrum. Methods Phys. Res. B: Beam Interact. Mater. Atoms **266**, 1533 (2008)
13. H. Ndilimabaka, S. Colis, G. Schmerber, D. Muller, J.J. Grob, L. Gravier, C. Jan, E. Beaurepaire, A. Dinia, Chem. Phys. Lett. **421**, 184 (2006)
14. C. Zhang, J. Phys. Chem. Solids **71**, 364 (2010)
15. A. Douayar, R. Diaz, F. Cherkaoui El Moursli, G. Schmerber, A. Dinia, M. Abd-Lefdil, Eur. Phys. J. Appl. Phys. **53**, 20501 (2011)
16. S.D. Shinde, G.E. Patil, D.D. Kajale, V.B. Gaikwad, G.H. Jain, J. Alloys Compd. **528**, 109 (2012)
17. M. Bouloudenine, N. Viart, S. Colis, A. Dinia, Catal. Today **113**, 240 (2006)
18. I. Soumahoro, G. Schmerber, A. Douayar, S. Colis, M. Abd-Lefdil, N. Hassanain, A. Berrada, D. Muller, A. Slaoui, H. Rinnert, A. Dinia, J. Appl. Phys. **109**, 33708 (2011)
19. J. Petersen, C. Brimont, M. Gallart, G. Schmerber, P. Gilliot, C. Ulhaq-Bouillet, J. L. Rehspringer, S. Colis, C. Becker, A. Slaoui, A. Dinia, J. Appl. Phys. **107**, 123522 (2010)
20. G.S. Chang, E.Z. Kurmaev, D.W. Boukhvalov, L.D. Finkelstein, A. Moewes, H. Bieber, S. Colis, A. Dinia, J. Phys. Condens. Matter **21**, 056002 (2009)
21. B. Roy, B. Karmakar, P.M.G. Nambissan, M. Pal, NANO: Brief Reports and Reviews **6**, 173 (2011)
22. M. Ungureanu, H. Schmidt, Q. Xu, H. von Wenckstern, D. Spemann, H. Hochmuth, M. Lorenz, M. Grundmann, Superlattices Microstruct. **42**, 231 (2007)

23. M. Subramanian, P. Thakur, S. Gautam, K.H. Chae, M. Tanemura, T. Hihara, S. Vijayalakshmi, S.S. Kim, K. Asokan, R. Jayavel, *J. Phys. D: Appl. Phys.* **42**, 105410 (2009)
24. R. Lardé, E. Talbot, P. Pareige, H. Bieber, G. Schmerber, S. Colis, V. Pierron-Bohnes, A. Dinia, *J. Am. Chem. Soc.* **133**, 1451 (2011)
25. S.R. Shinde, S.B. Ogale, J.S. Higgins, H. Zheng, A.J. Millis, V.N. Kulkarni, R. Ramesh, R.L. Greene, T. Venkatesan, *Phys. Rev. Lett.* **92**, 166601 (2004)
26. B. Roy, S. Chakrabarty, O. Mondal, M. Pal, A. Dutta, *Mater. Charact.* **70**, 1 (2012)
27. Y. Liu, W. Luo, R. Li, H. Zhu, X. Chen, *Optic Express* **17**, 9748 (2009)
28. A. Climent-Font, F. Pászti, G. García, M.T. Fernández-Jiménez, F. Agulló, *Nucl. Instr. Meth. B* **219-220**, 400 (2004)
29. H.-S. Cheng, H. Shen, J. Tang, F. Yang, *Nucl. Instr. Meth. B* **83**, 449 (1993)
30. M. Mayer, *SIMNRA User's Guide*, IPP 9/113 (1997)
31. F. Xian, X. Li, *Opt. Laser Technol.* **45**, 508 (2013)
32. S. Prabakar, M. Dhanam, *J. Cryst. Growth* **285**, 41 (2005)
33. S. Kahraman, F. Bayansal, H.A. Çetinkara, H.M. Çakmak, H.S. Güder, *Mater. Chem. Phys.* **134**, 1036 (2012)
34. R.D. Shannon, *Acta Cryst. A* **32**, 751 (1976)
35. J.H. Zheng, J.L. Song, Z. Zhao, Q. Jiang, J.S. Lian, *Cryst. Res. Technol.* **47**, 713 (2012)
36. Y. Belghazi, M. Ait Aouaj, M. El Yadari, G. Schmerber, C. Ulhaq-Bouillet, C. Leuvrey, S. Colis, M. Abd-lefdil, A. Berrada, A. Dinia, *Microelectronics* **40**, 265 (2009)
37. K.J. Kim, Y.R. Park, *Appl. Phys. Lett.* **81**, 1420 (2002)
38. V.R. Shinde, T.P. Gujar, C.D. Lokhande, R.S. Mane, S.H. Han, *Mater. Chem. Phys.* **96**, 326 (2006)
39. J. Petersen, C. Brimont, M. Gallart, O. Crégut, G. Schmerber, P. Gilliot, B. Hönerlage, C. Ulhaq-Bouillet, J. L. Rehspringer, C. Leuvrey, S. Colis, A. Slaoui, A. Dinia, *Microelectronics* **40**, 239 (2009)
40. H. Rinnert, P. Miska, M. Vergnat, G. Schmerber, S. Colis, A. Dinia, D. Muller, G. Ferblantier, A. Slaoui, *Appl. Phys. Lett.* **100**, 101908 (2012)